PAPER Special Section on Multidisciplinary and Innovative Key technologies in Advanced communication systems (MIKA)

Asynchronous NOMA Downlink Based on Single-Carrier Frequency-Domain Equalization

Tomonari KURAYAMA[†], ***Student Member***, **Teruyuki MIYAJIMA**[†a)], ***and*** **Yoshiki SUGITANI**[†], ***Members***

SUMMARY Non-orthogonal multiple access (NOMA) allows several users to multiplex in the power-domain to improve spectral efficiency. To further improve its performance, it is desirable to reduce inter-user interference (IUI). In this paper, we propose a downlink asynchronous NOMA (ANOMA) scheme applicable to frequency-selective channels. The proposed scheme introduces an intentional symbol offset between the multiplexed signals to reduce IUI, and it employs cyclic-prefixed single-carrier transmission with frequency-domain equalization (FDE) to reduce inter-symbol interference. We show that the mean square error for the FDE of the proposed ANOMA scheme is smaller than that of a conventional NOMA scheme. Simulation results show that the proposed ANOMA with appropriate power allocation achieves a better sum rate compared to the conventional NOMA.

key words: *asynchronous non-orthogonal multiple access, single-carrier transmission with frequency-domain equalization, frequency-selective channels, inter-user interference reduction*

1. Introduction

Non-orthogonal multiple-access (NOMA) has recently drawn significant interest for its ability to increase system throughput by allowing multiple users to share the same spectrum resource simultaneously [1]. Due to its attractive features, NOMA is a potential candidate for future wireless networks, where high spectral efficiency, massive connectivity, and low latency will be required to support various types of services [2]. In power-domain NOMA downlink, multiple signals are multiplexed at the base station (BS) and then separated at the user equipment (UE) based on the successive interference cancelation (SIC) principle [3]. As such, the interference among multiplexed signals, called inter-user interference (IUI), seriously limits the performance of NOMA.

To date, several studies have been conducted on the performance improvement of NOMA subject to IUI [4]. In [5], [6], multiple-antenna and beamforming techniques were employed to efficiently utilize spatial domain resources. In [7], the integration of NOMA and cooperative relaying was investigated to extend communication coverage. In [8], [9], resource allocation and user scheduling for NOMA were considered to improve spectral efficiency. Although these techniques can improve the performance of NOMA, they do not directly reduce IUI. If we can reduce IUI, we can expect further performance improvements.

Manuscript received November 8, 2021.
Manuscript revised February 10, 2022.
Manuscript publicized April 6, 2022.

[†]The authors are with the Graduate School of Science and Engineering, Ibaraki University, Hitachi-shi, 316-8511 Japan.
a) E-mail: teruyuki.miyajima.spc@vc.ibaraki.ac.jp

DOI: 10.1587/transcom.2021MEP0003

Recently, several attempts on a simple IUI reduction approach by asynchronous NOMA (ANOMA) have been made [10], [11]. In downlink ANOMA, an intentional symbol offset is introduced between the multiplexed signals at the BS. The idea of an intentional timing offset is not new, and it has been successfully applied to various communication scenarios [12], [13]. Also, in ANOMA, it was shown that the IUI component in the correlator output at a UE can be smaller than that in conventional synchronous NOMA [10], [11].

In [10], [11], the authors considered ANOMA in frequency-flat channels. When ANOMA is applied to wideband communications over frequency-selective channels, which are subject to inter-symbol interference (ISI), orthogonal frequency division multiplexing (OFDM) could be a natural choice to combat ISI. However, the ANOMA presented in [10], [11] cannot be applied to OFDM because the intentional symbol offset results in a phase shift and provides no IUI reduction. To overcome this issue, the authors in [14] considered intentional frequency offsets between the subcarriers of the multiplexed OFDM signals in frequency-flat channels and showed that IUI could be reduced. However, it is not clear how to apply this method to the case of frequency-selective channels. To the authors' knowledge, there have been no detailed studies on ANOMA applicable to frequency-selective channels.

In this paper, we propose a downlink ANOMA scheme in which single-carrier transmission with frequency domain equalization (SC-FDE) is adopted to enable the reduction of both IUI and ISI in frequency-selective channels instead of OFDM. We describe the FDE design based on the minimum mean square error (MMSE) criterion and demonstrate its superiority in terms of MSE performance compared to conventional synchronous NOMA. We also present a power allocation scheme that considers IUI reduction due to time asynchrony, and we show that it can help improve the sum rate through simulation.

Throughout this paper, we use the following notations: $(\cdot)^T$, $(\cdot)^H$, and $\|\cdot\|$ denote the transpose, Hermitian transpose, and norm of a vector or matrix, respectively. $\mathbb{E}[\cdot]$ represents the ensemble average. $\mathbf{I}_N$ denotes the $N \times N$ identity matrix. $[\mathbf{A}]_n$ and $[\mathbf{A}]_{n,n}$ denote the n-th row vector and (n,n)-th element of matrix $\mathbf{A}$, respectively. $(\mathbf{a})_n$ denotes the vector obtained by removing the n-th element of vector $\mathbf{a}$.

2. System Model

We consider a downlink ANOMA system consisting of a BS

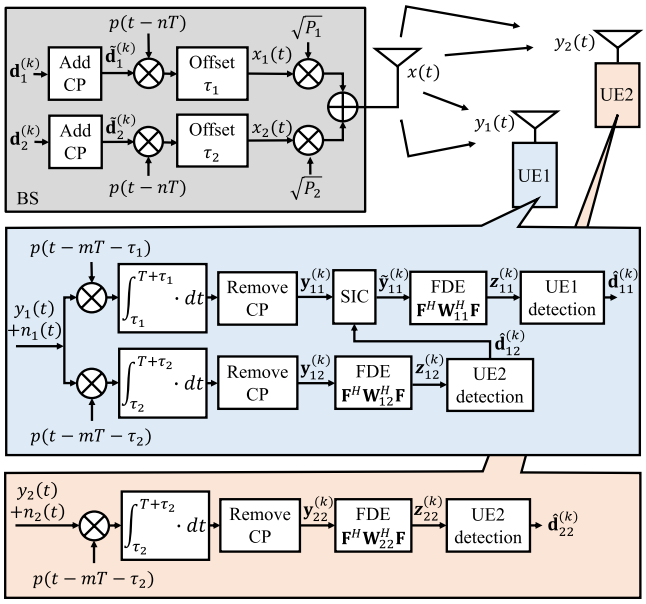

Fig. 1 Block diagram of the proposed downlink ANOMA scheme.

with a single antenna and two UEs, each equipped with a single antenna, as shown in Fig. 1. We assume that UE1 is closer to the BS than UE2 and uses SIC to remove the signal intended for UE2. We also assume that each channel between a UE and the BS is frequency-selective and modeled as a finite-impulse response filter. The BS and each UE have their perfect channel-state information. We employ the SC-FDE with cyclic prefix (CP) to compensate for the effect of the ISI caused by the channel.

2.1 Transmitter

Here, we explain the signal processing at the BS to send data symbols for each user. We form the k-th data symbol block for UEi as

$$\mathbf{d}_i^{(k)} \triangleq [d_{i,0}^{(k)} \cdots d_{i,N-1}^{(k)}]^T, \tag{1}$$

where N is the number of data symbols in a block, and $d_{i,n}^{(k)}$ is the n-th data symbol of the k-th block of UEi. We assume that the data symbols $d_{i,n}^{(k)}$ are normalized and independent of each other, i.e., $\mathbb{E}[d_{i,n}^{(k)} d_{i',n'}^{(k')*}] = 1$ for $k' = k, i' = i, n' = n$, and 0 otherwise. To avoid inter-block interference (IBI), a CP of length N_{CP} is added to the beginning of the transmission block $\mathbf{d}_i^{(k)}$. After adding the CP, the transmission block $\tilde{\mathbf{d}}_i^{(k)}$ can be represented as

$$\begin{aligned}\tilde{\mathbf{d}}_i^{(k)} &\triangleq [\tilde{d}_{i,kQ} \ \cdots \ \tilde{d}_{i,(k+1)Q-1}]^T \\ &= [d_{i,N-N_{\mathrm{CP}}}^{(k)} \cdots d_{i,N-1}^{(k)} \mid d_{i,0}^{(k)} \cdots d_{i,N-1}^{(k)}]^T,\end{aligned} \tag{2}$$

where $Q \triangleq N + N_{\mathrm{CP}}$.

Unlike NOMA, a different symbol offset is intentionally added to the transmitted signal for each UE before the signals are multiplexed in the power domain. We employ a real-valued unit energy pulse $p(t)$, which is limited to the interval

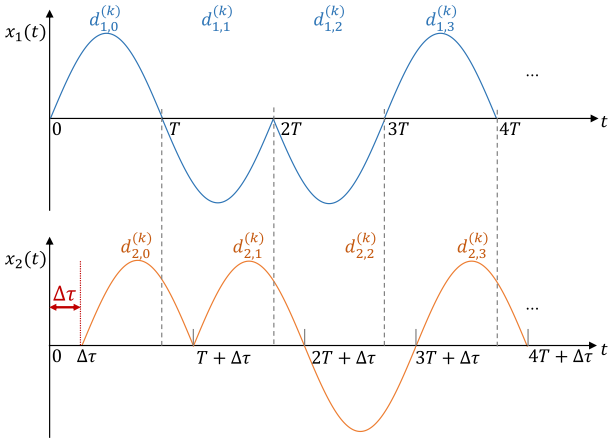

Fig. 2 Example of asynchronous transmission signals.

$[0, T]$. The reason for this limitation is to avoid IBI.

Then, the baseband continuous-time signal intended for UEi can be written as

$$x_i(t) = \sum_k \sum_{n=0}^{Q-1} \tilde{d}_{i,kQ+n} p(t - (kQ+n)T - \tau_i), \tag{3}$$

for $i = 1, 2$, where τ_i is the symbol offset, which is assumed to be $0 = \tau_1 < \tau_2 < T$ without loss of generality. Finally, two signals, $x_1(t)$ and $x_2(t)$, are multiplexed in the power domain and transmitted from the BS antenna. The multiplexed transmitted signal can be expressed as

$$x(t) = \sqrt{P_1} x_1(t) + \sqrt{P_2} x_2(t), \tag{4}$$

where P_i is the transmission power allocated to UEi. The total transmission power of the BS is denoted as $P \triangleq P_1 + P_2$.

Figure 2 shows an example of asynchronous transmission signals, where a half-sine pulse expressed as $p(t) = \sqrt{2}\sin(\pi t/T)$ for $0 \le t \le T$ and 0 otherwise [10] is used. In ANOMA, two signals with a symbol offset difference $\Delta\tau \triangleq \tau_2 - \tau_1$, $(0 < \Delta\tau < T)$ are multiplexed. Note that NOMA corresponds to $\Delta\tau = 0$.

2.2 Receivers

Here, we explain the signal processing at UEs to detect the data symbols. After $x(t)$ passes through a frequency-selective channel, the received signal at UEi is expressed as

$$y_i(t) = \sum_{l=0}^{L_i} h_{i,l} x(t - lT) + n_i(t), \tag{5}$$

where $h_{i,l}$ is the l-th coefficient of the impulse response of the communication channel between the BS and UEi of order L_i, and $n_i(t)$ is the additive white Gaussian noise at UEi with zero mean and power spectral density σ_i^2. The continuous-time received signal is processed by correlators to convert to discrete-time signals. Because UE1 performs SIC, it requires two correlators matched to $p(t-mT-\tau_1)$ and

$p(t-mT-\tau_2)$, while UE2 requires one correlator matched to $p(t-mT-\tau_2)$. In UEi, the output of the correlator matched to $p(t-mT-\tau_j)$ is expressed as

$$\begin{aligned} y_{ij,m} &= \int_{mT+\tau_j}^{(m+1)T+\tau_j} y_i(t)p(t-mT-\tau_j)dt \\ &= \sum_{l=0}^{L_i} h_{i,l}x_{j,m-l} + n_{ij,m}, \end{aligned} \tag{6}$$

for $i = 1, 2$, where

$$\begin{aligned} x_{1,m} &\triangleq \sqrt{P_1}\tilde{d}_{1,m} + \sqrt{P_2}(\rho_{\Delta\tau}\tilde{d}_{2,m} + \rho_{\Delta\tau-T}\tilde{d}_{2,m-1}), \\ x_{2,m} &\triangleq \sqrt{P_2}\tilde{d}_{2,m} + \sqrt{P_1}(\rho_{\Delta\tau}\tilde{d}_{1,m} + \rho_{\Delta\tau-T}\tilde{d}_{1,m+1}), \\ n_{ij,m} &\triangleq \int_{mT+\tau_j}^{(m+1)T+\tau_j} n_i(t)p(t-mT-\tau_j)dt, \\ \rho_{\Delta\tau} &\triangleq \int_0^T p(t)p(t-\Delta\tau)dt. \end{aligned} \tag{7}$$

In (7), $\rho_{\Delta\tau}$ is the autocorrelation of pulse $p(t)$. In $x_{j,m}$, the first and second terms correspond to the desired and IUI components, respectively. Unlike NOMA, where $x_{j,m} = \sqrt{P_1}\tilde{d}_{1,m} + \sqrt{P_2}\tilde{d}_{2,m}$, the IUI in $x_{j,m}$ is distributed over two consecutive symbols. As discussed later, the distributed nature of the IUI leads to a reduction in the overall IUI.

To avoid IBI, we assume that $L_i \le N_{\mathrm{CP}}$. After CP removal, the k-th received block consisting of the correlator outputs related to τ_j at UEi can be expressed as

$$\mathbf{y}_{ij}^{(k)} = \mathbf{H}_{\mathrm{cir},i}\mathbf{x}_j^{(k)} + \mathbf{n}_{ij}^{(k)}, \tag{8}$$

where

$$\begin{aligned} \mathbf{y}_{ij}^{(k)} &= [y_{ij,kQ+N_{\mathrm{CP}}} \ \cdots \ y_{ij,(k+1)Q-1}]^T, \\ \mathbf{x}_j^{(k)} &= [x_{j,kQ+N_{\mathrm{CP}}} \ \cdots \ x_{j,(k+1)Q-1}]^T, \\ \mathbf{n}_{ij}^{(k)} &= [n_{ij,kQ+N_{\mathrm{CP}}} \ \cdots \ n_{ij,(k+1)Q-1}]^T, \end{aligned}$$

and $\mathbf{H}_{\mathrm{cir},i} \in \mathbb{C}^{N\times N}$ is a circulant matrix consisting of $h_{i,l}$ defined by

$$\mathbf{H}_{\mathrm{cir},i} \triangleq \begin{bmatrix} h_{i,0} & & & h_{i,L_i} & \cdots & h_{i,1} \\ h_{i,1} & \ddots & & & \ddots & \vdots \\ \vdots & & \ddots & & & h_{i,L_i} \\ h_{i,L_i} & & & \ddots & & \\ & \ddots & & & \ddots & \\ & & h_{i,L_i} & \cdots & \cdots & h_{i,0} \end{bmatrix},$$

Note that due to the symbol offset, $d_{1,N-N_{\mathrm{CP}}}^{(k)}$ contained in the top of the current block $\mathbf{x}_1^{(k)}$ interferes with the previous block $\mathbf{x}_1^{(k-1)}$. To prevent this interference, although its influence is very small, we set $d_{1,N-N_{\mathrm{CP}}}^{(k)} = d_{1,0}^{(k-1)}$. Although this reduces the spectral efficiency, it is negligibly small for large N. As a result, we can express $\mathbf{x}_j^{(k)}$ as

$$\mathbf{x}_j^{(k)} = \begin{cases} \sqrt{P_1}\mathbf{d}_1^{(k)} + \sqrt{P_2}\bar{\mathbf{J}}\mathbf{d}_2^{(k)}, & j = 1, \\ \sqrt{P_2}\mathbf{d}_2^{(k)} + \sqrt{P_1}\mathbf{J}\mathbf{d}_1^{(k)}, & j = 2, \end{cases} \tag{9}$$

where

$$\begin{aligned} \mathbf{J} &\triangleq \rho_{\Delta\tau}\mathbf{I}_N + \rho_{\Delta\tau-T}\mathbf{T}, \\ \bar{\mathbf{J}} &\triangleq \rho_{\Delta\tau}\mathbf{I}_N + \rho_{\Delta\tau-T}\mathbf{T}^T, \\ \mathbf{T} &\triangleq \begin{bmatrix} 0 & 1 & & 0 \\ \vdots & & \ddots & \\ 0 & 0 & & 1 \\ 1 & 0 & \cdots & 0 \end{bmatrix}. \end{aligned}$$

At UEi, the data symbols of UE2 are detected using FDE, which reduces the effect of ISI. The FDE outputs are expressed as

$$\mathbf{z}_{i2}^{(k)} = \mathbf{F}^H\mathbf{W}_{i2}^H\mathbf{F}\mathbf{y}_{i2}^{(k)}, \tag{10}$$

where $\mathbf{F}$ is the N-point discrete Fourier transform matrix defined as

$$\begin{aligned} \mathbf{F} &\triangleq \frac{1}{\sqrt{N}}[\mathbf{f}_0 \cdots \mathbf{f}_{N-1}], \\ \mathbf{f}_k &\triangleq [e^{-j2\pi\frac{0\cdot k}{N}} \cdots e^{-j2\pi\frac{(N-1)\cdot k}{N}}]^T, \end{aligned}$$

and $\mathbf{W}_{ij}$ is the FDE matrix for UEj at UEi. The data detected from $\mathbf{z}_{i2}^{(k)}$ is denoted by $\hat{\mathbf{d}}_{i2}^{(k)}$. At UE1, the IUI replica generated by $\hat{\mathbf{d}}_{12}^{(k)}$ is subtracted from $\mathbf{y}_{11}^{(k)}$. Assuming that the SIC can cancel the IUI successfully, we obtain the IUI-free signal $\tilde{\mathbf{y}}_{11}^{(k)} = \mathbf{H}_{\mathrm{cir},1}\sqrt{P_1}\mathbf{d}_1^{(k)} + \mathbf{n}_{11}^{(k)}$. Finally, FDE is performed for UE1 as

$$\mathbf{z}_{11}^{(k)} = \mathbf{F}^H\mathbf{W}_{11}^H\mathbf{F}\tilde{\mathbf{y}}_{11}^{(k)}. \tag{11}$$

3. FDE Design

Next, we describe the FDE matrices $\mathbf{W}_{ij}$ based on the minimization of the following mean square error (MSE):

$$J_{ij} = \mathbb{E}\left[\|\mathbf{z}_{ij}^{(k)} - \sqrt{P_j}\mathbf{d}_j^{(k)}\|^2\right], \tag{12}$$

This criterion considers not only the compensation for ISI but also the reduction of IUI for $j = 2$.

Let us consider the optimal solution for UE2 ($j = 2$). Equation (12) can be rewritten as follows

$$\begin{aligned} J_{i2} &= \mathbb{E}\left[\|\mathbf{W}_{i2}^H\mathbf{F}\tilde{\mathbf{y}}_{i2}^{(k)} - \sqrt{P_2}\mathbf{F}\mathbf{d}_2^{(k)}\|^2\right] \\ &= \mathrm{Tr}\Big(P_2\mathbf{W}_{i2}^H\mathbf{F}\mathbf{H}_{\mathrm{cir},i}\mathbf{H}_{\mathrm{cir},i}^H\mathbf{F}^H\mathbf{W}_{i2}\Big) \\ &\quad + \mathrm{Tr}\Big(P_1\mathbf{W}_{i2}^H\mathbf{F}\mathbf{H}_{\mathrm{cir},i}\mathbf{R}\mathbf{H}_{\mathrm{cir,i}}^H\mathbf{F}^H\mathbf{W}_{i2}\Big) \\ &\quad - \mathrm{Tr}\Big(P_2\mathbf{W}_{i2}^H\mathbf{F}\mathbf{H}_{\mathrm{cir},i}\mathbf{F}^H\Big) - \mathrm{Tr}\Big(P_2\mathbf{F}\mathbf{H}_{\mathrm{cir},i}^H\mathbf{F}^H\mathbf{W}_{i2}\Big) \\ &\quad + \mathrm{Tr}\Big(P_2\mathbf{I}_N\Big) + \mathrm{Tr}\Big(\sigma^2\mathbf{W}_{i2}^H\mathbf{W}_{i2}\Big), \end{aligned} \tag{13}$$

where $\mathbf{R} \triangleq \mathbb{E}\left[\mathbf{J}\mathbf{d}_i^{(k)}(\mathbf{J}\mathbf{d}_i^{(k)})^H\right] = \mathbf{J}\mathbf{J}^H \in \mathbb{R}^{N\times N}$ becomes

$$\mathbf{R} = \begin{bmatrix} \rho_{\Delta\tau}^2+\rho_{\Delta\tau-T}^2 & \rho_{\Delta\tau}\rho_{\Delta\tau-T} & 0 & \cdots & \rho_{\Delta\tau}\rho_{\Delta\tau-T} \\ \rho_{\Delta\tau}\rho_{\Delta\tau-T} & \rho_{\Delta\tau}^2+\rho_{\Delta\tau-T}^2 & \rho_{\Delta\tau}\rho_{\Delta\tau-T} & 0 & 0 \\ 0 & \rho_{\Delta\tau}\rho_{\Delta\tau-T} & \rho_{\Delta\tau}^2+\rho_{\Delta\tau-T}^2 & \rho_{\Delta\tau}\rho_{\Delta\tau-T} & 0 \\ \vdots & \ddots & \ddots & \ddots & \vdots \\ 0 & 0 & \rho_{\Delta\tau}\rho_{\Delta\tau-T} & \rho_{\Delta\tau}^2+\rho_{\Delta\tau-T}^2 & \rho_{\Delta\tau}\rho_{\Delta\tau-T} \\ \rho_{\Delta\tau}\rho_{\Delta\tau-T} & \cdots & 0 & \rho_{\Delta\tau}\rho_{\Delta\tau-T} & \rho_{\Delta\tau}^2+\rho_{\Delta\tau-T}^2 \end{bmatrix}.$$

Note that $\mathbf{R}$ becomes the identity matrix in the case of NOMA. The FDE matrix $\mathbf{W}_{i2}$ that minimizes the MSE satisfies the following equation:

$$D_{\mathbf{W}_{i2}^*} J_{i2} = \left(P_2\mathbf{\Lambda}_i\mathbf{\Lambda}_i^H + P_1\mathbf{\Lambda}_i\mathbf{\Lambda}_\mathbf{R}\mathbf{\Lambda}_i^H + \sigma_i^2\mathbf{I}_N\right)\mathbf{W}_{i2} - P_2\mathbf{\Lambda}_i = \mathbf{0}, \quad (14)$$

where $D_{\mathbf{W}_{i2}^*}$ is the differential operator [17] with respect to $\mathbf{W}_{i2}^*$, $\mathbf{\Lambda}_i = \mathbf{F}\mathbf{H}_{\mathrm{cir},i}\mathbf{F}^H = \mathrm{diag}(H_{i,0}\cdots H_{i,N-1})$, and $H_{i,n}$ is the transfer function of the BS-UEi channel evaluated at the n-th subcarrier. $\mathbf{\Lambda}_\mathbf{R}$ is a diagonal matrix $\mathbf{\Lambda}_\mathbf{R} = \mathbf{F}\mathbf{R}\mathbf{F}^H = \mathrm{diag}(r_0\cdots r_{N-1})$ whose diagonal entry r_n is the eigenvalue of the circulant matrix $\mathbf{R}$, which is given by

$$r_n = (\rho_{\Delta\tau})^2 + (\rho_{\Delta\tau-T})^2 + 2\rho_{\Delta\tau}\rho_{\Delta\tau-T}\cos(2\pi n/N). \quad (15)$$

Solving (14), we obtain the optimum solution as

$$\mathbf{W}_{i2}^H = \mathbf{\Lambda}_i^H\left(\mathbf{\Lambda}_i\mathbf{\Lambda}_i^H + \frac{P_1}{P_2}\mathbf{\Lambda}_i\mathbf{\Lambda}_\mathbf{R}\mathbf{\Lambda}_i^H + \frac{\sigma_i^2}{P_2}\mathbf{I}_N\right)^{-1}. \quad (16)$$

For UE1 ($i = j = 1$), because the IUI component is removed by SIC, the FDE matrix reduces to

$$\mathbf{W}_{11}^H = \mathbf{\Lambda}_1^H\left(\mathbf{\Lambda}_1\mathbf{\Lambda}_1^H + \frac{\sigma_1^2}{P_1}\mathbf{I}_N\right)^{-1}. \quad (17)$$

Because all the matrices $\mathbf{W}_{ij}$ are diagonal, all the FDEs result in simple one-tap equalizers.

4. Power Allocation

Next, we consider power allocation among UEs. This problem has been well studied for NOMA [5], [15]. Here, we modify the power allocation scheme of [15], which maximizes the sum rate while satisfying the minimum required rate of each UE for application to the SC-FDE-based ANOMA. The scheme in [15] imposes the constraint $P_1 < P_2$ to achieve rate fairness between UEs under the assumption that UE1 is closer to the BS than UE2. The constraint ensures that the power of the IUI from UE1 is smaller than that of the desired UE2 component. In the following, we show that we can relax this constraint because the IUI power is reduced in ANOMA and derive the power allocation scheme under the relaxed constraint.

To this end, we need to analyze the relation between the IUI power in $\mathbf{z}_{12}$ for ANOMA, denoted by $P_{\mathrm{ANOMA}}^{\mathrm{IUI}}$, and that for NOMA, denoted by $P_{\mathrm{NOMA}}^{\mathrm{IUI}}$. The IUI power is defined by

$$P^{\mathrm{IUI}} \triangleq \mathbb{E}[\|\mathbf{F}^H\mathbf{W}_{12}^H\mathbf{F}\mathbf{H}_{\mathrm{cir},1}\sqrt{P_1}\mathbf{J}\mathbf{d}_1^{(k)}\|^2]/N. \quad (18)$$

Unfortunately, it is cumbersome to analyze the relation in the case of MMSE-based FDE because it depends on both $\rho_{\Delta\tau}$ and $\mathbf{H}_{\mathrm{cir},1}$. Therefore, we consider the case with zero-forcing (ZF)-based FDE $\mathbf{W}_{i2}^H = \mathbf{\Lambda}_i^{-1}$. In the case of NOMA, where $\mathbf{J} = \mathbf{I}_N$, the IUI power becomes $P_{\mathrm{NOMA}}^{\mathrm{IUI}} = \mathbb{E}[\|\mathbf{F}^H\mathbf{W}_{12}^H\mathbf{F}\mathbf{H}_{\mathrm{cir},1}\sqrt{P_1}\mathbf{d}_1^{(k)}\|^2]/N = P_1$. In the case of ANOMA, the IUI power is expressed as

$$P_{\mathrm{ANOMA}}^{\mathrm{IUI}} = \{(\rho_{\Delta\tau})^2 + (\rho_{\Delta\tau-T})^2\}P_1 = \beta P_{\mathrm{NOMA}}^{\mathrm{IUI}}, \quad (19)$$

where $\beta \triangleq (\rho_{\Delta\tau})^2 + (\rho_{\Delta\tau-T})^2$. We have a simple relation between $P_{\mathrm{ANOMA}}^{\mathrm{IUI}}$ and $P_{\mathrm{NOMA}}^{\mathrm{IUI}}$, which depends only on $\rho_{\Delta\tau}$. Because we have $\beta < 1$, as explained later, $P_{\mathrm{ANOMA}}^{\mathrm{IUI}}$ is smaller than $P_{\mathrm{NOMA}}^{\mathrm{IUI}}$. Owing to the IUI reduction in ANOMA, we can relax the power constraint as $\beta P_1 < P_2$.

We denote P_1 and P_2 as $P_1 = \alpha P$ and $P_2 = (1-\alpha)P$, where $0 \le \alpha \le 1$ is the power allocation ratio. The constraint for successful SIC decoding becomes $\alpha < \frac{1}{1+\beta}$ because $\beta P_1 < P_2 \Rightarrow \beta\alpha P < (1-\alpha)P$. The power allocation problem can be expressed as

$$\begin{aligned} &\max_{\alpha}\ R_1 + R_2, \\ &\text{s.t.}\quad R_i \ge \tilde{R}_i,\ 0 < \alpha < \bar{\alpha}, \end{aligned} \quad (20)$$

where $\bar{\alpha} = \frac{1}{1+\beta}$, $R_i = \log_2(1+\gamma_i)$ is the rate of UEi, $\tilde{R}_i$ is the minimum required rate of UEi, and γ_i is the signal-to-interference-plus-noise ratio (SINR) for any $0 \le n \le N-1$ are expressed as

$$\gamma_1 \triangleq \frac{\alpha P_1^{\mathrm{des}}}{\alpha P_1^{\mathrm{ISI}} + P_1^{\mathrm{noise}}}, \quad (21)$$

$$\gamma_2 \triangleq \frac{(1-\alpha)P_2^{\mathrm{des}}}{(1-\alpha)P_2^{\mathrm{ISI}} + \alpha P_2^{\mathrm{IUI}} + P_2^{\mathrm{noise}}}, \quad (22)$$

where $P_i^{\mathrm{des}} \triangleq P|[\mathbf{G}_i]_{n,n}|^2$, $P_i^{\mathrm{ISI}} \triangleq P\|([\mathbf{G}_i]_n)_n\|^2$, $P_i^{\mathrm{noise}} \triangleq \sigma_i^2\|[\mathbf{V}_i]_n\|^2$, $P_2^{\mathrm{IUI}} \triangleq P[\mathbf{G}_2]_n\mathbf{R}[\mathbf{G}_2]_n^H$, $\mathbf{G}_i \triangleq \mathbf{V}_i\mathbf{H}_{\mathrm{cir},i}$, and $\mathbf{V}_i \triangleq \mathbf{F}^H\mathbf{W}_{ii}^H\mathbf{F}$. Because the optimization problem (20) is convex, it can be solved by the Karush–Kuhn–Tucker (KKT) condition [16]. Consequently, the optimal power allocation ratio α_{opt} can be obtained as follows:

$$\alpha_{\mathrm{opt}} = \begin{cases} \alpha_0, & \alpha_1 < \alpha_0 < \min\{\alpha_2, \bar{\alpha}\} \\ \alpha_1, & \alpha_0 \le \alpha_1 < \bar{\alpha} \\ \alpha_2, & \alpha_2 \le \alpha_0 \ \text{ and } \ \alpha_2 < \bar{\alpha} \end{cases} \quad (23)$$

where α_0 is the power allocation ratio that maximizes the sum rate $f(\alpha) = R_1 + R_2$, and $\alpha_i, i = 1,2$ are the values that achieve the minimum required rate for UEi, i.e., $R_i = \tilde{R}_i$. Note that $\tilde{R}_i$ in (20) has to be selected such that $\alpha_1 \le \alpha_2$ is satisfied for the existence of α_{opt}. We provide the derivation of (23) in the Appendix.

5. MSE Analysis

We analyzed the performance of the SC-FDE-based ANOMA by comparing the SC-FDE-based NOMA with the MMSE-based FDE in (16). Here, we consider the MSE J_{i2}

in (12) at the FDE outputs of UE2 at UEi. In the case of ANOMA, the MSE reduces to

$$J_{\mathrm{ANOMA}} = P_2 \sum_{n=0}^{N-1} \left\{ 1 - \frac{|H_{i,n}|^2 P_2}{|H_{i,n}|^2(P_2 + P_1 r_n) + \sigma_i^2} \right\}. \tag{24}$$

Also, the MSE of the NOMA J_{NOMA} is obtained by setting $r_n = 1, \forall n$ in (24). Then, we obtain the following result on the superiority of the SC-FDE-based ANOMA over the NOMA:

Proposition 1: Given P_i and $H_{i,n}$, $J_{\mathrm{NOMA}} > J_{\mathrm{ANOMA}}$ holds for any $\Delta\tau$.

Proof : The difference between the MSEs of NOMA and ANOMA can be expressed as $J_{\mathrm{NOMA}} - J_{\mathrm{ANOMA}} = \sum_{n=0}^{N-1} J_n^{\mathrm{diff}}$, where J_n^{diff} is

$$J_n^{\mathrm{diff}} = \frac{P_1 P_2^2 |H_{i,n}|^2 (1 - r_n) / \{|H_{i,n}|^2 (P_2 + P_1) + \sigma_i^2\}}{|H_{i,n}|^2 (P_2 + P_1 r_n) + \sigma_i^2}. \tag{25}$$

When $\rho_{\Delta\tau}\rho_{\Delta\tau-T} > 0$, (15) shows that $(\rho_{\Delta\tau} - \rho_{\Delta\tau-T})^2 \le r_n \le (\rho_{\Delta\tau} + \rho_{\Delta\tau-T})^2$. From (7), we have

$$(\rho_{\Delta\tau} + \rho_{\Delta\tau-T})^2 = \left(\int_0^T p(t) g(t) dt \right)^2, \tag{26}$$

where $g(t) = p(t-\Delta\tau) + p(t+T-\Delta\tau)$ is $p(t)$ circularly shifted by $\Delta\tau$. Thus, we have $\int_0^T g(t)^2 dt = 1$. Then, we can obtain $(\rho_{\Delta\tau} + \rho_{\Delta\tau-T})^2 \le 1$ using Schwarz's inequality. This results in $0 \le r_n \le 1$, and thus $J_n^{\mathrm{diff}} \ge 0, \forall n$. Because the equality holds if and only if $n = 0$, we can obtain $\sum_{n=0}^{N-1} J_n^{\mathrm{diff}} > 0$. When $\rho_{\Delta\tau}\rho_{\Delta\tau-T} < 0$, we obtain the same result. □

Note that it can be derived from the above discussion that $\beta = (\rho_{\Delta\tau})^2 + (\rho_{\Delta\tau-T})^2$ in (19) is smaller than 1.

Next, we have the following result for $\Delta\tau$ that minimizes J_{ANOMA}:

Proposition 2: J_{ANOMA} is minimized when $\Delta\tau = T/2$ if $\rho_{\Delta\tau} > 0$ and $\rho_{\Delta\tau}$ monotonically decreases with $\Delta\tau$.

Proof : From (15), we have

$$\begin{aligned} r_n = {} & (\rho_{\Delta\tau} - \rho_{\Delta\tau-T})^2 \sin^2(\pi n/N) \\ & + (\rho_{\Delta\tau} + \rho_{\Delta\tau-T})^2 \cos^2(\pi n/N), \quad \forall n \end{aligned} \tag{27}$$

From the inequality of arithmetic and geometric means, r_n is minimized when $\rho_{\Delta\tau} = \rho_{\Delta\tau-T}$. Then, we have

$$\int_{\Delta\tau}^{T} p(t) p(t - \Delta\tau) dt = \int_{T-\Delta\tau}^{T} p(t) p(t - (T - \Delta\tau)) dt. \tag{28}$$

Clearly, this equality holds if $\Delta\tau = T - \Delta\tau$, which is equivalent to $\Delta\tau = T/2$. Because $\rho_{\Delta\tau}(\rho_{\Delta\tau-T})$ monotonically decreases (increases) with $\Delta\tau$, $\rho_{\Delta\tau} = \rho_{\Delta\tau-T}$ holds only if $\Delta\tau = T/2$. From (24), J_{ANOMA} is minimized when r_n is minimized. □

In the simulation presented in the next section, we employed two pulse shapes: a rectangular pulse of $p(t) = 1$ for $0 \le t \le T$ and 0 otherwise and the half-sine pulse [10]. These pulses satisfy the conditions on $\rho_{\Delta\tau}$ in Proposition 2.

6. Simulation Results

Computer simulations were conducted to evaluate the performance of the proposed ANOMA and compare it with conventional NOMA and OMA, which is a two-time slot time-division multiple-access scheme. Unless otherwise stated, the simulation settings were as follows: $N = 2^6$, $P = 30$ dBm, $L_1 = L_2 = 3$, $\sigma_i^2 = -103$ dBm, and $\tau_1 = 0$. The coefficients of the channel impulse responses were $h_{i,l} \in \mathcal{CN}(0, \tilde{\sigma}_l^2)$ and $\tilde{\sigma}_l^2 = \lambda \exp(-\eta l), l = \{0, \cdots, L_i\}$, where $\lambda = G_i / \sum_{l=0}^{L_i} \exp(-\eta l)$ with $\eta = 0.23$. The path loss model used was $G_i = 128.1 + 37.6 \log_{10} \tilde{r}_i$ dB, where $\tilde{r}_i$ km is the distance between the BS and the UEi [18]. $\tilde{r}_1 = 0.15, \tilde{r}_2 = 0.3$. The minimum required rate was set as the rate of the OMA defined by $\tilde{R}_i = \frac{1}{2} \log_2(1 + \gamma_i^{\mathrm{OMA}})$.

Figure 3 shows the MSE of UE2 as a function of the symbol offset difference $\Delta\tau$. We assumed fixed power allocation $P_1 = P_2 = P/2$ to see the improvement achieved by the symbol offset. We observed that the MSE of ANOMA was always lower than that of NOMA. In addition, the MSE could be reduced by properly setting the symbol offset, and it was minimized at $\Delta\tau = T/2$, which agrees with our analysis. The half-sine pulse provided better performance than the rectangular pulse when $0.3T \le \Delta\tau \le 0.7T$.

Figure 4 shows the average SINR γ_2 of UE2 as a function of the symbol offset difference $\Delta\tau$, where $P_1 = P_2 = P/2$. We observed that the SINR of ANOMA was higher than that of NOMA. This is because IUI was efficiently reduced by the symbol offset. As in Fig. 3, the effect of the symbol offset is maximized at $\Delta\tau = T/2$ for both pulses.

Figure 5 shows the autocorrelation $\rho_{\Delta\tau}$ of the pulses and $\beta = (\rho_{\Delta\tau})^2 + (\rho_{\Delta\tau-T})^2$ as a function of the symbol offset difference $\Delta\tau$. From Figs. 4 and 5, SINR is large when

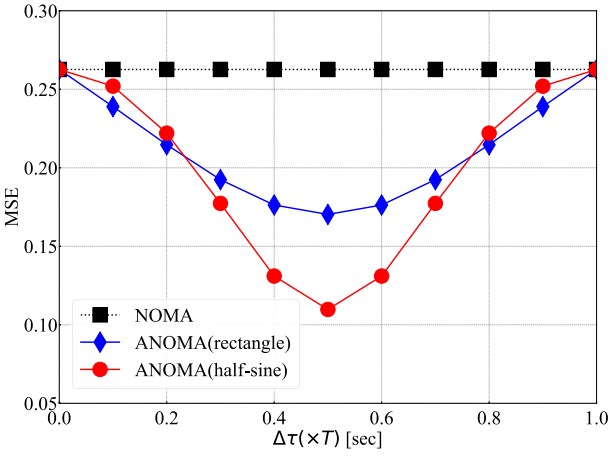

Fig. 3 Effect of symbol offset on MSE of UE2.

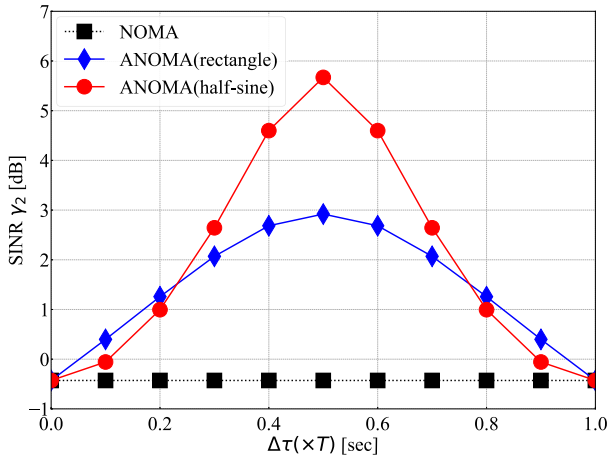

Fig. 4 Effect of symbol offset on average SINR of UE2.

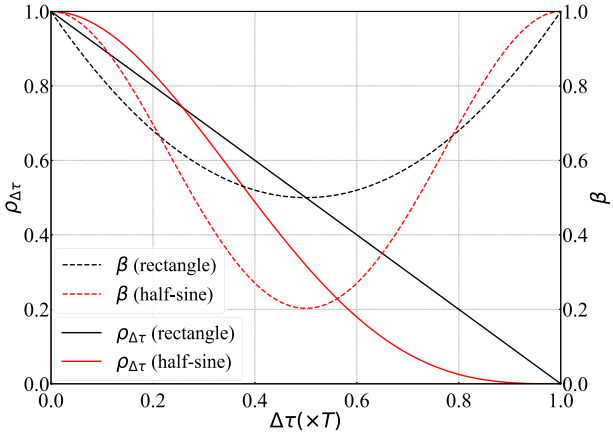

Fig. 5 Effect of symbol offset on $\rho_{\Delta\tau}$ and β.

β is small, and vice versa. Although a rigorous analysis of the relation between SINR and β is difficult when the MMSE-based FDE is used, we can derive the SINR when the ZF-based FDE is used. The SINR can be written as $\gamma_2^{\mathrm{ZF}} = \frac{(1-\alpha)P}{\beta\alpha P + P_2^{\mathrm{noise}}}$. This clarifies that the SINR improves as β decreases.

Figures 6 and 7 show the achievable rate regions when the rectangular pulse and the half-sine pulse were used, respectively, when $\Delta\tau = T/2$. It can be seen that ANOMA could achieve a larger rate region than NOMA and OMA. In addition, the performance of the half-sine pulse was better than that of the rectangular pulse.

In the following simulations, we used the half-sine pulse and $\Delta\tau = T/2$. Figure 8 shows the achievable rate of each UEi as a function of the BS transmission power P. Both UEs of ANOMA had higher rates than NOMA and OMA. As the transmit power P increased, the improvements were more evident.

Finally, we examined the effect of the power allocation scheme. Figure 9 shows an example of the sum rate characteristics against the power allocation ratio α. The characteristics of the NOMA are also shown, where $\alpha_{\mathrm{X}}^{\mathrm{NOMA}}$s

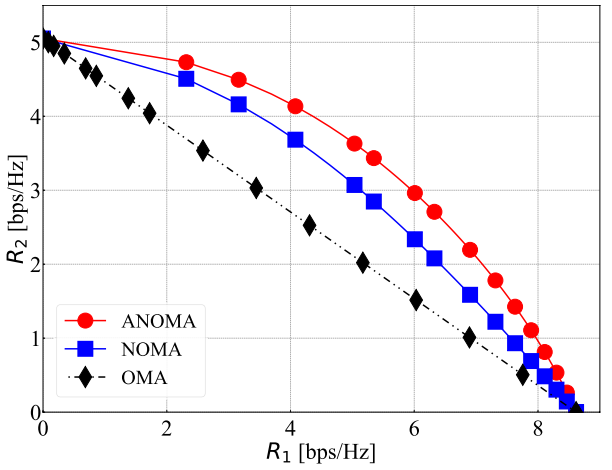

Fig. 6 Achievable rate regions (rectangle, $\Delta\tau = 0.5$).

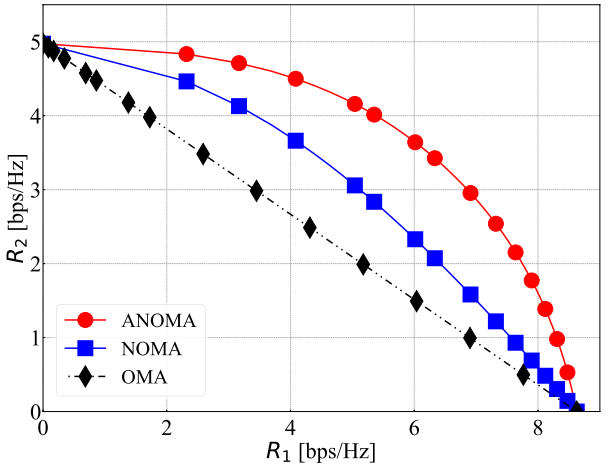

Fig. 7 Achievable rate regions (half-sine, $\Delta\tau = 0.5$).

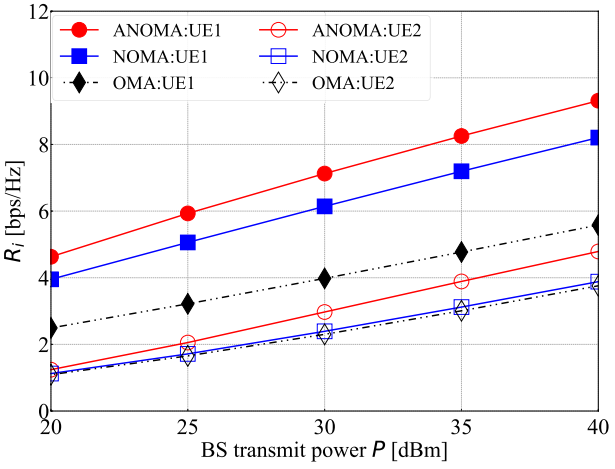

Fig. 8 Achievable rate of each UE ($\Delta\tau = 0.5$).

were obtained by (23) with $\bar{\alpha} = 0.5$. In ANOMA, the selected ratio α_{opt} is identical to α_0, which maximizes the sum rate, because the range $\mathcal{I}$ within which α is constrained is

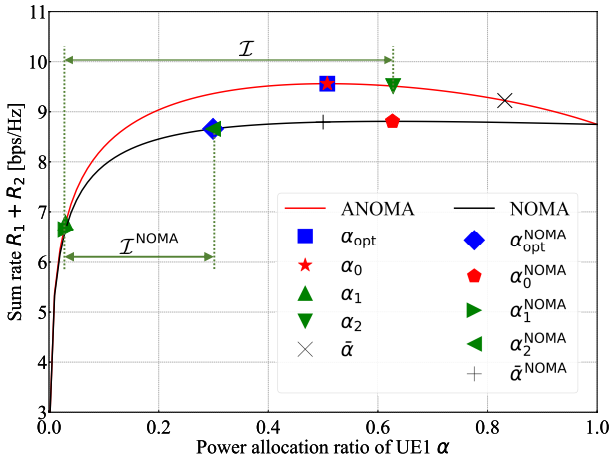

Fig. 9 Effect of power allocation ratio α on sum rate ($\Delta\tau = 0.5$).

sufficiently wide to include α_0. In NOMA, $\alpha_{\mathrm{opt}}^{\mathrm{NOMA}}$ is not identical to α_0^{NOMA} because of the narrower range $\mathcal{I}^{\mathrm{NOMA}}$. We found that the optimum value of α_{opt} was larger than $\alpha_{\mathrm{opt}}^{\mathrm{NOMA}}$, and the resulting sum rate increased by allocating more power to the near-user UE1.

7. Conclusion

In this paper, we proposed a downlink ANOMA scheme based on SC-FDE to enable IUI reduction, even in the presence of ISI. MSE analysis showed that ANOMA outperforms NOMA, and the best performance was achieved when the symbol offset difference was $\Delta\tau = T/2$ for some pulse shapes. Simulation results showed that ANOMA with appropriate power allocation can provide a superior sum rate compared to NOMA and OMA.

We assumed that a pulse $p(t)$ is limited to the interval $[0,T]$ to avoid IBI. From the practical point of view, it is worth investigating the application of pulses whose support is not limited to $[0,T]$ [11]. The performance of ANOMA depends on the autocorrelation $\rho_{\Delta\tau}$, which is closely related to the spectrum of the used pulse. Thus, further investigation is desired to clarify the effect of the spectrum of the pulses to the performance of the proposed ANOMA.

Acknowledgments

The study was supported by JSPS KAKENHI Grant Number JP20K04479.

References

[1] Y. Saito, Y. Kishiyama, A. Benjenbbour, T. Nakamura, A. Li, and K. Higuchi, "Non-orthogonal multiple access (NOMA) for cellular future radio access," Proc. IEEE Veh. Technol. Conf. (VTC Spring), Dresden, Germany, pp.1–5, June 2013.
[2] W. Saad, M. Bennis, and M. Chen, "A vision of 6G wireless systems: Applications, trends, technologies, and open research problems," IEEE Netw., vol.34, no.3, pp.134–142, May 2020.
[3] K. Higuchi and A. Benjebbour, "Non-orthogonal multiple access (NOMA) with successive interference cancellation for future radio access," IEICE Trans. Commun., vol.E98-B, no.3, pp.403–414, March 2015.
[4] S.M.R. Islam, N. Avazov, O.A. Dobre, and K.-S. Kwak, "Power-domain non-orthogonal multiple access (NOMA) in 5G systems: Potentials and challenges," IEEE Commun. Surveys Tuts., vol.19, no.2, pp.721–742, 2nd Quart., 2017.
[5] B. Kim, S. Lim, H. Kim, S. Suh, J. Kwun, S. Choi, C. Lee, S. Lee, and D. Hong, "Non-orthogonal multiple access in downlink multiuser beam forming system," Proc. IEEE Milit. Commun. Conf. (MILCOM), San Diego, CA, USA, pp.1278–1283, Nov. 2013.
[6] Z. Ding, F. Adachi, and H.V. Poor, "The application of MIMO to non-orthogonal multiple access," IEEE Trans. Wireless Commun., vol.15, no.1, pp.537–552, Jan. 2016.
[7] M. Zeng, W. Hao, O.A. Dobre, and Z. Ding, "Cooperative NOMA: State of the art, key techniques, and open challenges," IEEE Netw., vol.34, no.5, pp.205–211, July 2020.
[8] X. Li, C. Li, and Y. Jin, "Dynamic resource allocation for transmit power minimization in OFDM-based NOMA system," IEEE Commun. Lett., vol.20, no.12, pp.2558–2561, Dec. 2016.
[9] J. Cui, Y. Liu, Z. Ding, P. Fan, and A. Nallanathan, "Optimal user scheduling and power allocation for millimeter wave NOMA systems," IEEE Trans. Wireless Commun., vol.17, no.3, pp.1502–1517, March 2018.
[10] J. Cui, G. Dong, S. Zhang, H. Li, and G. Feng, "Asynchronous NOMA for downlink transmissions," IEEE Commun. Lett., vol.21, no.2, pp.402–405, Feb. 2017.
[11] M. Ganji and H. Jafarkhani, "Time asynchronous NOMA for downlink transmission," Proc. IEEE Wireless Commun. Netw. Conf. (WCNC), Marrakesh, Morocco, pp.1–6, April 2019.
[12] A. Das and B.D. Rao, "MIMO systems with intentional timing offset," EURASIP J. Adv. Signal Process., vol.2011, no.1, pp.1–14, Dec. 2011.
[13] M. Ganji and H. Jafarkhani, "Interference mitigation using asynchronous transmission and sampling diversity," Proc. IEEE Global Commun. Conf. (GLOBECOM), Washington, DC, USA, pp.1–6, Dec. 2016.
[14] M. Ganji and H. Jafarkhani, "Improving NOMA multi-carrier systems with intentional frequency offsets," IEEE Wireless Commun. Lett., vol.8, no.4, pp.1060–1063, Aug. 2019.
[15] C.L. Wang, J.Y. Chen, and Y.J. Chen, "Power allocation for a downlink non-orthogonal multiple access system," IEEE Wireless Commun. Lett., vol.5, no.5, pp.532–535, Oct. 2016.
[16] S. Boyd, and L. Vandenberghe, Convex Optimization, Cambridge University Press, 2004.
[17] A. Hjørungnes and D. Gesbert, "Complex-valued matrix differentiation: Techniques and key results," IEEE Trans. Signal Process., vol.55, no.6, pp.2740–2746, June 2007.
[18] 3GPP, TR 25.942 V3.3.0 (2002-06), RF System Scenarios, June 2002.

Appendix: Derivation of (23)

First, we obtain the power allocation ratios α_i satisfying $R_i = \tilde{R}_i$ for $i = 1, 2$ as

$$\alpha_1 = \frac{P_1^{\mathrm{noise}}}{P_1^{\mathrm{des}}/(2^{\tilde{R}_1} - 1) - P_1^{\mathrm{ISI}}}, \tag{A·1}$$

$$\alpha_2 = \frac{P_2^{\mathrm{des}}/(2^{\tilde{R}_2} - 1) - P_2^{\mathrm{ISI}} - P_2^{\mathrm{noise}}}{P_2^{\mathrm{des}}/(2^{\tilde{R}_2} - 1) - P_2^{\mathrm{ISI}} + P_2^{\mathrm{IUI}}}. \tag{A·2}$$

Also, we can obtain the ratio α_0 satisfying $D_\alpha f(\alpha) = 0$ as

$$\alpha_0 = \frac{\sqrt{B^2 + AC} - B}{A}, \tag{A·3}$$

where D_α is the differential operator with respect to α, and $A > 0, B > 0, C > 0$ are defined as

$$\begin{aligned} A &= P_1^{\mathrm{ISI}} P_2^{\mathrm{des}} (P_2^{\mathrm{IUI}} + P_1^{\mathrm{des}})(P_2^{\mathrm{des}} + P_2^{\mathrm{ISI}}) \\ &\quad + P_1^{\mathrm{des}} P_1^{\mathrm{noise}} (P_2^{\mathrm{des}} + P_2^{\mathrm{ISI}} - P_2^{\mathrm{IUI}})(P_2^{\mathrm{IUI}} - P_2^{\mathrm{ISI}}), \\ B &= P_1^{\mathrm{noise}} \{ P_2^{\mathrm{des}} P_1^{\mathrm{ISI}} (P_2^{\mathrm{IUI}} + P_2^{\mathrm{nosie}}) \\ &\quad + P_1^{\mathrm{des}} (P_2^{\mathrm{des}} + P_2^{\mathrm{ISI}} - P_2^{\mathrm{IUI}})(P_2^{\mathrm{ISI}} + P_2^{\mathrm{noise}}) \}, \\ C &= P_1^{\mathrm{noise}} \{ P_1^{\mathrm{des}} (P_2^{\mathrm{des}} + P_2^{\mathrm{IUI}} + P_2^{\mathrm{noise}})(P_2^{\mathrm{ISI}} + P_2^{\mathrm{noise}}) \\ &\quad - P_2^{\mathrm{des}} P_1^{\mathrm{noise}} (P_2^{\mathrm{IUI}} + P_2^{\mathrm{noise}}) \}. \end{aligned}$$

Next, we derive the KKT conditions [16] for (20) as follows:

$$\begin{aligned} &\text{i)} \quad -D_\alpha f(\alpha) + \mu_1 D_\alpha g_1(\alpha) + \mu_2 D_\alpha g_2(\alpha) = 0, \\ &\text{ii)} \quad \mu_1 g_1(\alpha) = 0, \quad \text{iii)} \quad \mu_2 g_2(\alpha) = 0, \\ &\text{iv)} \quad \mu_1 \geq 0, \quad \text{v)} \quad \mu_2 \geq 0, \\ &\text{vi)} \quad g_1(\alpha) \leq 0, \quad \text{vii)} \quad g_2(\alpha) \leq 0, \\ &\text{viii)} \quad 0 < \alpha < \bar{\alpha}, \end{aligned}$$

where $f(\alpha) = R_1 + R_2, g_i(\alpha) = \tilde{R}_i - R_i$, and μ_i is a Lagrangian coefficient.

When $\mu_1 > 0$ and $\mu_2 = 0$, the solution α_{opt} satisfies $g_1(\alpha_{\mathrm{opt}}) = 0$ from ii). Thus, we have

$$\alpha_{\mathrm{opt}} = \alpha_1. \tag{A·4}$$

Because the ratio α_{opt} satisfies $g_2(\alpha_{\mathrm{opt}}) < 0$ from vii) and $\alpha_{\mathrm{opt}} < \bar{\alpha}$ from viii), we obtain the following condition:

$$\alpha_{\mathrm{opt}} < \min\{\alpha_2, \bar{\alpha}\}. \tag{A·5}$$

When $\mu_1 = 0$ and $\mu_2 > 0$, the solution α_{opt} satisfies $g_2(\alpha_{\mathrm{opt}}) = 0$ from iii). Then, we have

$$\alpha_{\mathrm{opt}} = \alpha_2. \tag{A·6}$$

Because the ratio α_{opt} satisfies $g_1(\alpha_{\mathrm{opt}}) < 0$ from vi) and $\alpha_{\mathrm{opt}} < \bar{\alpha}$ from viii), we obtain the following condition:

$$\alpha_1 < \alpha_{\mathrm{opt}} < \bar{\alpha}. \tag{A·7}$$

When $\mu_1 > 0$ and $\mu_2 > 0$, the solution α_{opt} satisfies $g_1(\alpha_{\mathrm{opt}}) = g_2(\alpha_{\mathrm{opt}}) = 0$ from ii) and iii). This leads to

$$\alpha_{\mathrm{opt}} = \alpha_1 = \alpha_2. \tag{A·8}$$

From viii), we obtain the following condition:

$$\alpha_{\mathrm{opt}} < \bar{\alpha}. \tag{A·9}$$

When $\mu_1 = \mu_2 = 0$, the solution α_{opt} satisfies $D_\alpha f(\alpha_{\mathrm{opt}}) = 0$ from i). Then, we obtain

$$\alpha_{\mathrm{opt}} = \alpha_0. \tag{A·10}$$

Because $g_1(\alpha_0) < 0$ and $g_2(\alpha_0) < 0$ from vi) and vii), we obtain the following condition:

$$\alpha_1 < \alpha_{\mathrm{opt}} < \min\{\alpha_2, \bar{\alpha}\}, \tag{A·11}$$

From (A·5), (A·7), (A·8), and (A·11), the following condition has to be satisfied for the existence of a solution:

$$\alpha_1 \leq \alpha_2. \tag{A·12}$$

Then, note that the case of (A·4) occurs when $\alpha_0 \leq \alpha_1$, and the case of (A·6) occurs when $\alpha_2 \leq \alpha_0$. Summarizing the above results, we obtain (23).

Tomonari Kurayama received B.Eng. and M.Eng. in electrical and electronic engineering from Ibaraki University, Hitachi, Japan in 2020 and 2022, respectively. In 2022, he joined DOCOMO CS Tokai, Ink., Nagoya, Japan. His research interests include signal processing for wireless communications.

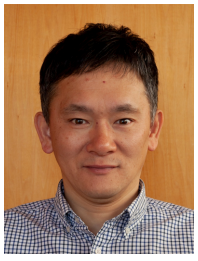

Teruyuki Miyajima received B.Eng., M.Eng., and Ph.D. in electrical engineering from Saitama University, Saitama, Japan, in 1989, 1991, and 1994, respectively. In 1994, he joined Ibaraki University, Hitachi, Japan, where he is currently a professor in the domain of electrical and electronic systems engineering. His current interests include signal processing for wireless communications. Dr. Miyajima is a member of IEEE.

Yoshiki Sugitani received M.Eng. and Ph.D. in electrical engineering from Osaka Prefecture University, Sakai, Japan, in 2013 and 2016, respectively. In 2016, he joined Ibaraki University, Hitachi, Japan, where he is currently a lecturer in the domain of electrical and electronic systems engineering. His current interests include control for the synchronization of complex networks. Dr. Sugitani is a member of IEICE.